Improvement of As(III) removal with diatomite overlay nanoscale zero-valent iron (nZVI-D): adsorption isotherm and adsorption kinetic studies

Nusavadee Pojananukij, Kitirote Wantala, Sutasinee Neramittagapong, Chitsan Lin, Duangkanok Tanangteerpong and Arthit Neramittagapong

ABSTRACT

Nanoscale zero-valent iron coated on diatomite (nZVI-D) was successfully synthesized as a composite material. It is the combination of nZVI and diatomite which has been proved to be a promising material in arsenite or As(III) removal. The result showed that 25.5% of As(III) was removed using diatomite only but more than 95% of As(III) was removed using nZVI-D, at the same contact time of 60 min and pH 6. The experimental isotherm data for As(III) adsorption at different initial concentrations were analyzed using the Langmuir, Freundlich, and Dubinin–Radushkevich equations. Among these three, the equilibrium data fitted well with the Langmuir isotherm. The kinetic adsorption was also studied using the pseudo-first, second-order, and intraparticle diffusion equations. The data were well explained by the pseudo-second-order kinetic model. From the results of kinetic adsorption and the adsorption isotherm, it can be concluded that arsenite adsorption was controlled by the mass transfer and adsorption process.

Key words | adsorption isotherm, arsenite (As(III)), diatomite, kinetic studies, nZVI-D

Nusavadee Pojananukij
Kitirote Wantala
Sutasinee Neramittagapong
Duangkanok Tanangteerpong
Arthit Neramittagapong (corresponding author)
Department of Chemical Engineering, Faculty of Engineering,
Khon Kaen University,
Khon Kaen 40002, Thailand
E-mail: *artner@kku.ac.th*

Kitirote Wantala
Sutasinee Neramittagapong
Duangkanok Tanangteerpong
Arthit Neramittagapong
Research Center for Environmental and Hazardous Substance Management (EHSM), Faculty of Engineering,
Khon Kaen University,
Khon Kaen 40002, Thailand

Chitsan Lin
Department of Marine Environmental Engineering,
National Kaohsiung Marine University,
Kaohsiung 81157, Taiwan

INTRODUCTION

The presence of heavy metal ions in the environment is worrying because of the dangerous effects on human and animal health. Arsenic is one of the most toxic heavy metals and can cause lung, liver, kidney and bladder cancers if accumulated in the body. Arsenic compounds have been classified as Group I carcinogens (Straif *et al.* 2009) and therefore, the maximum contamination limit for arsenic in drinking water is reported to be below 10 μg/L by the World Health Organization (WHO 2010). The natural processes for the environmental spreading of arsenic are weathering reactions such as biological activities and volcanic emissions as well as human activities like mining, petroleum refineries and ceramic manufacturing industries (Mahmood *et al.* 2012). As(III) in water is commonly found in the form of inorganic species at neutral pH and exists as the uncharged species H_3AsO_3 (Kanel *et al.* 2006). It is well known that the toxicity of As(III) is higher than As(V) and it has been reported that it is more difficult to treat compared to As(V) (Çiftçi & Henden 2015).

Recently, several methods have been used to treat As(III) contamination in drinking water such as precipitation, electrochemical reduction, adsorption, ion exchange, and reverse osmosis (Manning *et al.* 2002). However, these methods are costly and have limitations when treating the metals at low concentration. Modification of clay minerals has been proposed to significantly remove some inorganic compounds (Pan *et al.* 2010). One modification method is to make a stable negative charge on the surface of mineral clays to exchange electrons

doi: 10.2166/ws.2016.120

with an inorganic compound and thus enhance adsorption of heavy metals such as As(III) (Zhang *et al.* 2010). Several researchers have investigated the adsorption of heavy metal on mineral clays, especially using diatomite (Al-Degs *et al.* 2001; Pan *et al.* 2010). Diatomite ($SiO_2 \cdot nH_2O$) is a natural amorphous siliceous mineral in clay. It is relatively soft, lightweight with a porous structure and is composed of aquatic unicellular alga. Diatomite is considered suitable as a supporting material according to its catalysis property, containing negatively charged ions, low cost and ease of purchase.

Many reports have indicated that nanoscale zero-valent iron (nZVI) can treat environmental contaminants such as heavy metals due to its large, active surface area, high adsorption capacity and oxidation reaction process (Yun *et al.* 2013). Moreover, nZVI has been utilized to treat arsenic contamination in an aqueous environment (Hokkanen *et al.* 2015). Thus, it would be very interesting to load nZVI onto the diatomite surface in order to eliminate As(III) in drinking water.

This research was focused on the synthesis and characterization of nZVI on diatomite and also on studying the efficiency of As(III) removal from aqueous solution using this nZVI-D composite. The study of batch adsorption was carried out to investigate the influence of initial concentration and contact time on As(III) removal. Finally, the adsorption model and isotherms were used to describe the kinetic adsorption process of As(III) removal by nZVI-D.

MATERIALS AND METHODS

Materials

All chemicals used in this study were analytical grade and all stock solutions were prepared with deionized water from Millipore Milli-Q equipment (resistivity of 18 MΩ cm). The As(III) stock solutions were prepared by dissolving sodium arsenite ($NaAsO_2$, Ajax Finechem, New Zealand) in DI water. Iron(III) sulfate ($FeSO_4 \cdot 7H_2O$, Ajax Finechem, New Zealand) and sodium borohydride ($NaBH_4$, Rankem, India) were utilized to synthesize the nanoscale zero-valent iron coated on diatomite (nZVI-D) by reduction methods. Natural diatomite received from north Thailand was used as the support of nZVI particles in this study. Additionally, 1 and 0.1 M sodium hydroxide (NaOH, Panreac, Barcelona) and hydrochloric acid (HCl, RCL Labscan, Thailand) were used to adjust the solution pH.

Preparation of nZVI-D

The diatomite was washed with distilled water and dried in an oven at 105 °C for 24 h. About 10 g of dry diatomite was mixed with 100 mL of 1 M $FeSO_4 \cdot 7H_2O$. It was then dried at 110 °C in the oven and washed with deionized water. The solid was iron-oxide-coated diatomite (IOCD) and was used to prepare nZVI-D in further experiments. The nZVI-D was prepared by adding 50 mL of 0.1 M $NaBH_4$ with a dropping rate of 2 mL/min into the IOCD at 25 °C, and then the mixture was stirred for 30 minutes. The nZVI particles appeared after the first drop of $NaBH_4$ solution. After 30 min of agitation, the nZVI-D was separated and washed with methanol (once) and ID water (twice), and then the nZVI-D was dried with nitrogen gas at 70 °C and stored in a desiccator.

Characterization

The chemical composition of diatomite and nZVI-D was investigated using X-ray fluorescence (XRF-1700, Shimadzu Co., Japan). The specific surface area was measured by an N_2 adsorption–desorption instrument (ASAP 2010, Micromeritics, USA) and calculated by the Brunauer–Emmett–Teller analytical technique. The morphologies of diatomite and nZVI-D were observed by the transmittance electron microscopy (TEM) technique (TECNAI G2 20S–TWIN, FEI, Czech Republic). The nZVI suspension was deposited on a 400-mesh copper grid (Electron Microscopy Sciences, Hatfield, PA) and air-dried. The samples were prepared by depositing a few droplets of dilute nanoparticle solution onto a carbon film prior to transmission electron microscopy.

Effect of adsorbent and contact time

Two different adsorption types of 0.75 g/L were prepared by mixing 0.09 g of adsorbent in 120 mL of 1,000 μg/L As(III) concentration using a mechanical magnetic stirrer at a speed of 160 rpm. The effect of adsorbent type at different contact times was studied until the removal efficiency (%) was constant. The experiment was conducted in pH 6 solution which was adjusted by adding a few drops of

0.1 M of HCl or NaOH and a pH meter was used to measure the pH.

Equilibrium and adsorption kinetics

An amount of 0.09 g of nZVI-D was added in a conical flask containing 120 mL of As(III) to obtain 0.75 g/L nZVI-D. The equilibrium experiment was conducted by using the prepared 0.75 g/L nZVI-D to adsorb the solution at different initial concentrations of 1,000, 1,250, 1,500, 1,750, and 2,000 μg/L. The initial pH of the solution was adjusted to 6 with 0.1 M of HCl or NaOH. During the adsorption, the conical flask was covered with aluminum foil to prevent the oxidation of As(III). The mixture was shaken by a mechanical magnetic stirrer at a speed of 160 rpm and 30 °C for 1, 3, 5, 10, 20, 30 and 60 min. After that, the suspensions were filtered through a 0.45 μm nylon syringe filter. The As(III) residual concentration was analyzed using a graphite furnace atomic absorption spectrometer (GFAAS, Perkin Elmer series Analyst 880, USA). Each experiment was carried out in triplicate and the mean value was reported.

The removal efficiency of arsenite (%) and the adsorption capacity (q_t in μg/g) were determined as follows:

$$\text{Removal efficiency}(\%) = \left(\frac{C_0 - C_t}{C_0}\right) \times 100 \quad (1)$$

$$\text{Adsorption capacity } (q_t) = \left(\frac{C_0 - C_t}{M}\right) \times V \quad (2)$$

where C_0 and C_t are the initial concentration and concentration at the time of arsenite in the solution (μg/L), respectively. V is the volume of the solution (L), and M is the mass of adsorbent (g).

Adsorption isotherm models

The experimental data of adsorption isotherms were fitted with several models: Freundlich, Langmuir, and Dubinin–Radushkevich (D–R) isotherms. These models were used to describe the relationship between the adsorbed amount of As(III) and its equilibrium concentration in the solution.

The Freundlich isotherm (as shown in Equation (3)) is an empirical equation. It can be applied to the non-uniform distribution of adsorption heat and affinities over a heterogeneous surface.

$$\log q_e = \log K_F + \frac{1}{n} \log C_e \quad (3)$$

where C_e is the equilibrium concentration of adsorbate (mg/L), q_e is the amount of metal adsorbed per gram of the adsorbent at equilibrium (mg/g), K_F is the Freundlich isotherm constant (mg/g) and n is the adsorption intensity.

The Langmuir isotherm describes quantitatively the formation of a monolayer on the outer surface of the adsorbent with a finite number of identical sites. The model assumes uniform energies of adsorption onto the surface.

$$\frac{C_e}{q_e} = \frac{C_e}{q_m} + \frac{1}{q_m K_L} \quad (4)$$

where q_m is the maximum monolayer coverage capacity (mg/g) and K_L is the Langmuir isotherm constant (L/mg).

The D–R isotherm model is a semi-empirical equation used to estimate the porosity of each adsorbent and the free energy of adsorption. It assumes that the adsorption was on a heterogeneous surface, involving van der Waals forces, and is applied for physical adsorption processes. The D–R isotherm model is expressed as:

$$\ln q_e = \ln q_d - \beta \varepsilon^2 \quad (5)$$

where q_d is the D–R constant (mg/g) and β is the constant related to free energy.

Adsorption kinetics

Adsorption kinetics depend on the adsorbate–adsorbent interactions and operating conditions. Several kinetic models are used to examine the controlling mechanisms of adsorption processes, e.g. chemical reaction, diffusion control, and mass transfer. In this study, the adsorption equilibrium data were analyzed using three kinetic models: pseudo-first-order, pseudo-second-order and intra-particle diffusion.

The pseudo-first-order kinetic model is a widely known one describing the adsorption rate based on solid capacity.

It is generally expressed as follows:

$$\ln(q_e - q_t) = \ln q_e - k_1 t \quad (6)$$

where q_e and q_t are the adsorption capacity at equilibrium and at time t, respectively (mg/g), and k_1 is the rate constant of pseudo-first-order adsorption (min^{-1}).

The pseudo-second-order kinetic model is based on solid phase adsorption and is expressed as follows:

$$\frac{t}{q_t} = \frac{1}{k_2 q_e^2} + \frac{1}{q_e} t \quad (7)$$

where k_2 (g/μg·min) is the pseudo-second-order rate constant of adsorption.

The intra-particle diffusion model explains the resistance of intra-particle diffusion affecting adsorption and is generally represented as follows:

$$q_t = k_i t^{1/2} \quad (8)$$

Table 1 | Chemical compositions of natural diatomite and nZVI-D

Formula	Diatomite (%)	nZVI-D (%)
SiO_2	79.76	48.40
Fe_2O_3	2.49	11.10
Al_2O_3	9.61	7.65
K_2O	0.74	1.16
TiO_2	0.17	0.38
MgO	0.85	0.19

where k_i (μg/g·$min^{1/2}$) is the intra-particle diffusion rate constant.

RESULTS AND DISCUSSION

Characterization of diatomite and nZVI-D

The X-ray fluorescence analyses of diatomite and nZVI-D samples are presented in Table 1. The main chemical compositions of both samples consisted of SiO_2, Al_2O_3, Fe_2O_3, MgO, TiO_2 and K_2O. The difference of 8.61% observed in the amount of Fe_2O_3 in nZVI and nZVI-D corresponds to the amount of nZVI attached to diatomite. The SEM image of diatomite highlights the cylindrical shape of particles with the structure of pores on the surface as shown in Figure 1(a). After n-ZVI was added onto diatomite, there was some partial coverage and pore blocking on the surface of diatomite as shown in Figure 1(b). TEM images of diatomite and nZVI-D are shown in Figure 2(a) and 2(b). It can be seen that some nanoparticles were attached and dispersed on the inner surface of diatomite and some of the nZVI was covered on the outer surface of diatomite. The nZVI appeared as a spherical particle and formed a slightly chain-like aggregate (Prasad *et al.* 2014) with the particle size ranging between 50 and 80 nm.

Effect of adsorbent type and contact time

The effect of adsorbent (diatomite and nZVI-D) on As(III) adsorption was studied by using an initial As(III) concentration

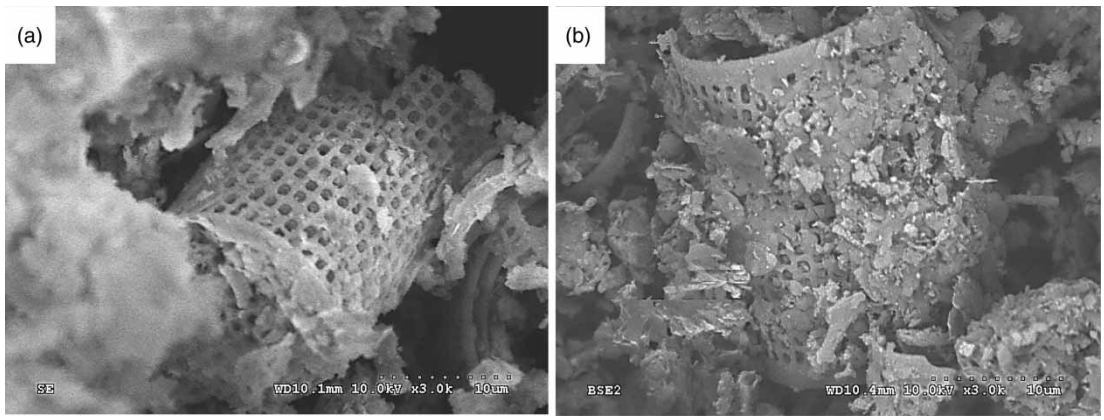

Figure 1 | SEM images of (a) diatomite and (b) nZVI supported on diatomite (nZVI-D).

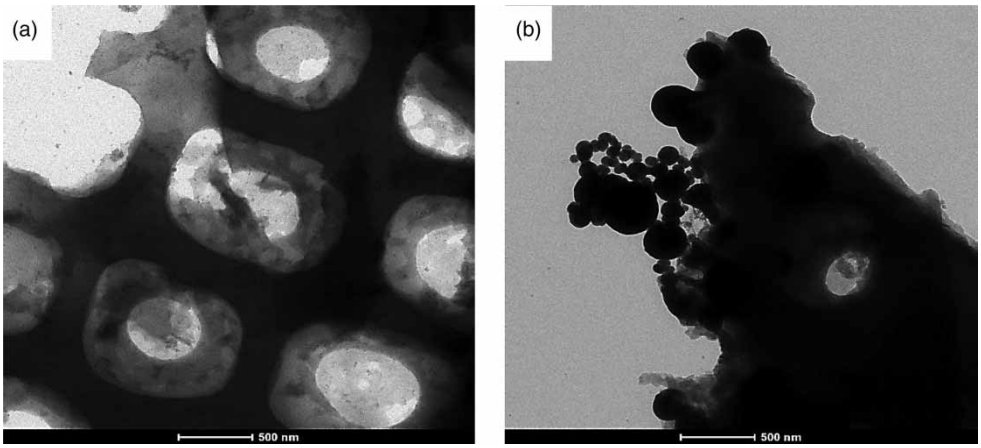

Figure 2 | TEM images of (a) diatomite and (b) nZVI supported on diatomite (nZVI-D).

of 1,000 μg/L at 30 °C and pH 6. It can be seen in Figure 3 that the diatomite can only remove As(III) by 25.50% but the nZVI-D can remove up to 96.16% in aqueous solution within 60 min, which is about four times higher. The enhanced effectiveness of the nZVI-D for As(III) removal was due to nZVI forming on the surface of diatomite and, therefore, reacting with As(III) in the solution (Yan *et al.* 2012). Moreover, the removal efficiency of As (III) increased with contact time, and reached equilibrium by 10 and 20 mins, on diatomite and nZVI-D, respectively. This was thought to be because most of the available sites on the adsorbents (diatomite and nZVI-D) were saturated with As(III) and, hence, the adsorbents reached the maximum point of As (III) adsorption. A high As(III) adsorption rate between 0 and

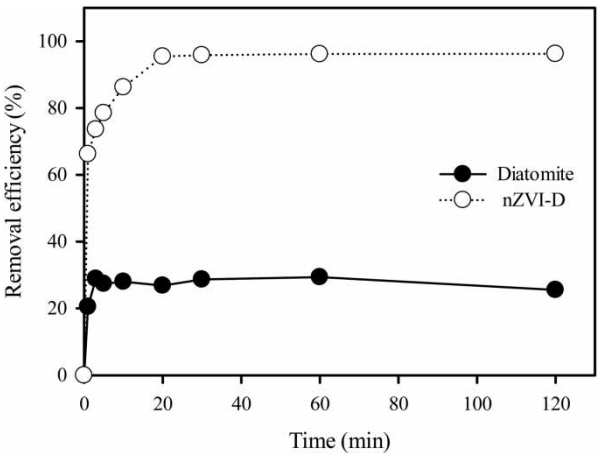

Figure 3 | Effect of adsorbent type at different contact times on As(III) removal at the initial concentration of As(III) of 1,000 μg/L using 0.75 g/L of diatomite and nZVI-D at initial pH 6 and 30 °C.

10 mins was observed and this was thought to be due to the high concentration gradient between the bulk solution and the solid–liquid interface that leads to a high driving force of adsorption. After 20 min, the As(III) removal rate was slower, which was due to less diffusion of As(III) to the inside surface of the adsorbent (Jiang *et al.* 2009). The subsequent experiments on the nZVI-D adsorbent were therefore carried out using a contact time of 60 min. At an initial As(III) concentration of 1,000 μg/L, the synthesized nZVI-D could not remove As(III) as low as the allowable concentration in drinking water of 10 μg/L. However, if 0.75 g/L of adsorbent dose and the initial As(III) concentration of 500 μg/L were used, the nZVI-D could remove As(III) down to below 10 μg/L within 60 min, which meets the World Health Organization (WHO) standard for arsenic concentration in drinking water of 10 μg/L (data not shown). Therefore, nZVI-D was chosen for studying the adsorption isotherm and adsorption kinetics.

Effect of initial concentration

The effect of initial As(III) concentration on the removal efficiency and adsorption capacity of nZVI-D were investigated. The conditions in this study were determined as a contact time of 60 min and pH 6. Figure 4(a) shows the removal efficiency (calculated from Equation (1)) of As(III) at initial concentrations of 1,000, 1,250, 1,500, 1,750 and 2,000 μg/L. It was found that the lowest initial As(III) concentration resulted in the highest removal efficiency of 96%. It can be seen that the As(III) removal efficiencies decreased with an increase of the

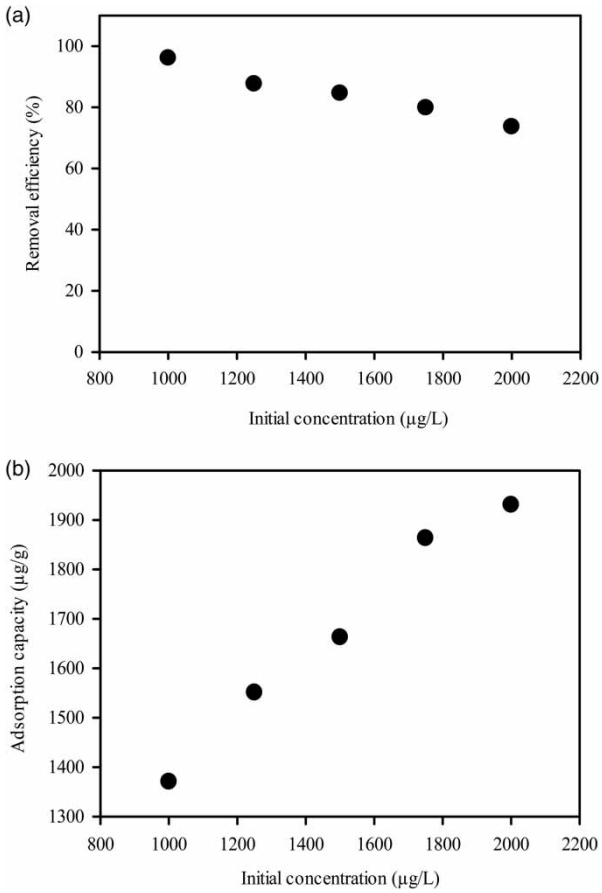

Figure 4 | Effect of initial concentration on As(III) removal: (a) removal efficiency, (b) adsorption capacity by 0.75 g/L of nZVI-D at initial pH 6.

initial As(III) concentrations due to the lack of available active sites on the surface of these adsorbents (Lv *et al.* 2012). This is consistent with the results of the adsorption capacity calculated from Equation (2) (Figure 4(b)), which found that the adsorption capacity increased with As(III) concentrations. However, the adsorption capacity in the initial concentration ranging between 1,800 and 2,000 μg/L was not significant because the active sites on the nZVI-D were not enough to adsorb As(III). It can be seen that at higher concentrations the active sites of nZVI-D became more saturated and adsorption capacity approached a constant value (Al-Ghouti *et al.* 2009).

Adsorption isotherms

Three isotherm models, namely Freundlich, Langmuir and D–R, were used to describe the equilibrium data of As(III) on nZVI-D. The Freundlich isotherm, Langmuir isotherm and D–R parameters are displayed in Table 2. It can be seen that the experimental data of As(III) adsorption by nZVI-D can be well fitted with Langmuir adsorption isotherms due to high correlation coefficients ($R^2 = 0.99$), more than those of the Freundlich ($R^2 = 0.95$) and D–R ($R^2 = 0.65$) adsorption isotherms. Therefore, the removal of As(III) by nZVI-D implied that a monolayer (chemisorption) of As(III) covered the surface of the adsorbent and that the surface contained a finite number of particular adsorption sites (Karagöz *et al.* 2008). The maximum adsorption capacity (q_m) was 2,734 μg/g and R_L of the Langmuir isotherm was 0.025–0.044, which was obtained from the intercept of the plots of C_e/q_e versus C_e, at a different initial concentration (Table 2). The R_L value of the Langmuir isotherm in a range of 0–1 indicates the nature of the adsorption process (Monash & Pugazhenthi 2009), therefore, R_L in the study was in the range of 0–1, which indicated a favorable adsorption process for As(III) on the nZVI-D surface. It can also be concluded that the effect of the initial concentration affected the absorption rate, but that this is not a linear relationship, that is, when the initial concentration is doubled, adsorption capacity to absorb will not be doubled. The correlation coefficient of the D–R isotherm is lower than that of the Freundlich and Langmuir isotherms, suggesting that the As(III) adsorption onto nZVI-D is not a physical process.

Table 2 | The values of different adsorption isotherms for As(III) adsorption of nZVI-D at different As(III) initial concentrations ranging between 1,000 and 2,000 μg/L (temperature: 30 °C, 0.75 g/L of nZVI-D, initial pH 6)

Langmuir constants		Freundlich constants		D–R constants	
q_m (μg/g)	2,734.49	n	7.05	q_D (mg/g)	1,830.12
K_L (L/mg)	0.0201	K_F ((μg/g)•(L/μg)$^{1/n}$)	706.15	β	8.12×10^{-5}
R_L	0.025–0.044	R^2	0.948	E	7.85
R^2	0.994			R^2	0.647

The maximum adsorption capacity of As(III) (q_m) on nZVI-D at the initial concentrations ranging between 1,000 and 2,000 μg/L was 2,734 μg/g (Table 2). This is much higher than the maximum adsorption capacity of other adsorbents reported in the literature, for instance Al-HDTMA-sericite (852 μg/g) (Tiwari & Lee 2012), Al-AMBA-sericite (541 μg/g) (Tiwari & Lee 2012), activated alumina (76 μg/g) (Singh & Pant 2004) and Fe-hydrotalcite-supported magnetite nanoparticles (12 μg/g) (Zhang *et al.* 2013).

Adsorption kinetics

The kinetics of the adsorption process were evaluated by fitting the experimental data with the pseudo-first-order and pseudo-second-order models. The values obtained from the models are shown in Table 3. It was found that the experimental kinetic data fitted the pseudo-second-order ($R^2 = 0.998$) better than the pseudo-first-order ($R^2 = 0.952$). Thus, the pseudo-second-order kinetic model is more likely to describe the overall rate of the adsorption process of As(III) on nZVI-D. Based on pseudo-second-order kinetic model ascription, chemical adsorption involves the valence electron forces shared between the adsorbent and heavy metal (Erdem *et al.* 2016). In addition, the values of k_2 (Figure 5(a)) decreased with the increase of initial As(III) concentration (1,000–1,500 μg/L) and became constant at 1,750–2,000 μg/L. It is shown that when the initial concentrations increased, the adsorption constant rate (k_2) between 1,750 and 2,000 μg/L was not significant. A high driving force of high concentration was thought to affect the adsorption rate. However, the absorption rate obtained from this experiment was not consistent with the absorption theory because the active sites of the absorbent were limited. Therefore, Figure 5(b) was plotted in order to explain the adsorption capacity of the active sites. It can be seen that the available active sites of absorbent decreased with the increase of initial concentration. Furthermore, more than 95% of the active site was used to absorb As(III) at an initial concentration of 1,750μg/L. The low value of k_2 (between 1,750 and 2,000 μg/L) displayed in Figure 5(a) may indicate that the surface of the absorbent at high concentration was covered by As(III) particles, which is demonstrated by a small change of q_t/q_m in Figure 5(b).

Effect of mass transfer

The determination of the rate-limiting step is important for understanding the adsorption process. The pseudo-first-order and pseudo-second-order models cannot explain the rate-limiting step during the adsorption process; therefore, the intra-particle diffusion model was used to explain the diffusion of the adsorbate molecules into the pores and to find a suitable kinetic model for the process. If the plot of q_t versus $t^{1/2}$ is a straight line and passes through the origin, the adsorption process is controlled by intra-particle diffusion only. However, if the line does not pass through the origin, intra-particle diffusion was not the only

Table 3 | Adsorption kinetic model rate constants for As(III) adsorption on nZVI-D at different initial concentrations (temperature: 30 °C; 0.75 g/L of nZVI-D, initial pH 6)

C_0 (μg/L)	1,000	1,250	1,500	1,750	2,000
$q_{e,\exp}$ (μg/g)	1,827.60	2,068.16	2,216.90	2,484.22	2,574.35
Pseudo-first-order					
$q_{e,\mathrm{cal}}$ (μg/g)	657.66	590.28	661.69	903.52	1,013.94
k_1 (L/min)	0.175	0.120	0.121	0.124	0.108
R^2	0.952	0.877	0.849	0.920	0.941
Pseudo-second-order					
$q_{e,\mathrm{cal}}$ (μg/g)	1,378.43	1,521.45	1,658.85	1,865.77	1,857.52
$k_2 \times 10^{-3}$ (g/μg·min)	1.05	1.30	0.93	0.61	0.60
R^2	0.995	0.998	0.997	0.995	0.993
Intra-particle diffusion					
k_{i1} (μg/g·min$^{1/2}$)	133.06	198.15	278.08	302.99	246.70
k_{i2} (μg/g·min$^{1/2}$)	6.69	15.86	13.18	11.97	23.41

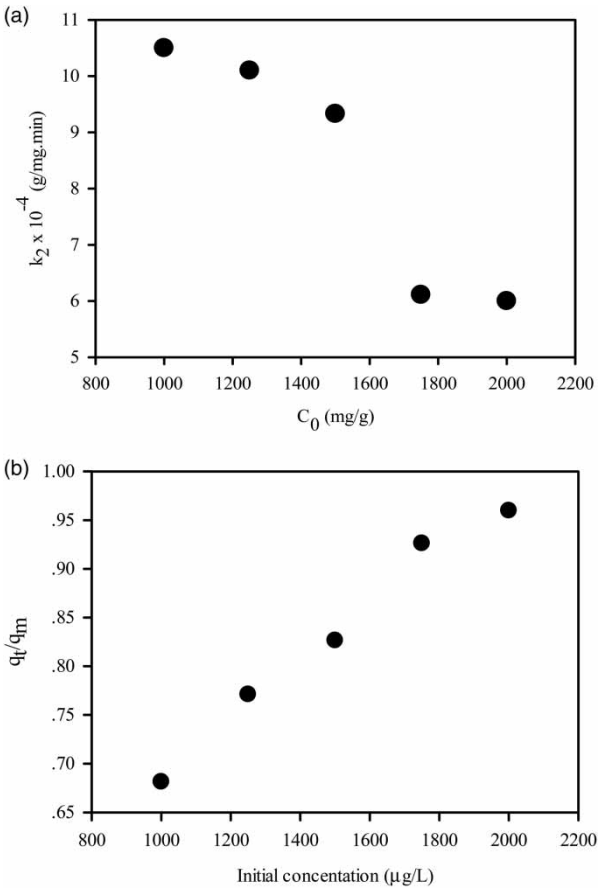

Figure 5 | (a) Rate constant (k_2) of pseudo-second-order adsorption (g/µg·min) and (b) experimental adsorption capacity per maximum adsorption capacity (q_t/q_m) of nZVI-D at various As(III) initial concentrations (C_0 between 1,000 and 2,000 µg/L).

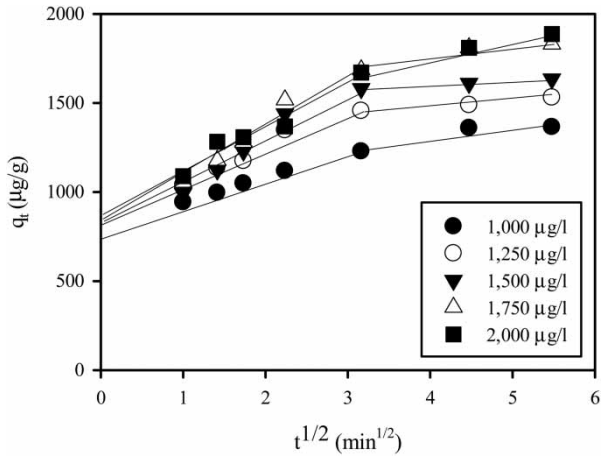

Figure 6 | Adsorption capacity of As(III) fitted with the intra-particle diffusion model onto nZVI-D (0.75 g/L of nZVI-D at initial pH 6) for various As(III) initial concentrations at $t^{1/2}$ (min$^{1/2}$).

rate-determining step. The total adsorption rate can be described by three steps in general adsorption (Pojananukij *et al.* 2015): (1) film or surface diffusion of solution is transported from the bulk solution into the external surface of the adsorbent; (2) the solution molecules move into the interior of the adsorbent particles (intra-particle or pore diffusion); and (3) adsorption on the interior sites of the adsorbent.

Figure 6 shows the intra-particle diffusion plots of Equation (8) for the As(III) adsorption into the nZVI-D. It was observed that the linear plots did not pass through the origin, which indicates that intra-particle diffusion was not the only rate-controlling step. In addition, it is apparent that more than one linear slope appeared in all of the plots, which indicates that the adsorption process was affected by more than one diffusion phenomenon (Vaghetti *et al.* 2008). The external diffusion can be determined by the first slope (k_{i1}), while the intra-particle diffusion can be evaluated by another slope. As shown in Figure 6 and Table 3 at the initial concentration of 1,000 µg/L, the diffusion rate constants for external (k_{i1}) and internal (k_{i2}) mass transfer were found to be 133.06 and 6.69 µg/g·min$^{1/2}$, respectively. Therefore, the intraparticle diffusion could be a rate-determining step.

From the kinetic and mass transfer studies, it can be inferred that intra-particle diffusion between As(III) and nZVI-D had a significant effect on adsorption and that the adsorption processes were chemical adsorption.

CONCLUSIONS

Nanoscale zero-valent iron coated on diatomite has been successfully used as an effective adsorbent for As(III) removal in contaminated water sources. As(III) removal efficiency decreased with the increase of initial concentration. The Langmuir isotherm showed a better fit than the Freundlich isotherm and D–R, thus indicating that adsorption involved the formation of a monolayer and a heterogeneous surface of As(III) particles covered the surface of the adsorbent. The maximum adsorption capacity for the adsorption of As(III) onto nZVI-D was found to be 2,734.49 µg/g. The pseudo-first-order and pseudo-second-order kinetic models have been used to describe the adsorption kinetics. However, the pseudo-second-order was a more accurate and

suitable model due to a higher correlation coefficient (R^2), and therefore the adsorption process was found to be chemisorption. The rate-controlling step may be controlled by film diffusion and intra-particle diffusion.

ACKNOWLEDGEMENTS

This research was financially supported by the Research Fund for Supporting Lecturer to Admit High Potential Student to Study and Research on His Expert Program Year 2012, 551T212, Khon Kaen University.

REFERENCES

Al-Degs, Y., Khraisheh, M. A. M. & Tutunji, M. F. 2001 Sorption of lead ions on diatomite and manganese oxides modified diatomite. *Water Res.* **35** (15), 3724–3728.

Al-Ghouti, M. A., Khraisheh, M. A. M., Ahmad, M. N. M. & Allen, S. 2009 Adsorption behaviour of methylene blue onto Jordanian diatomite: a kinetic study. *J. Hazard. Mater.* **165** (1–3), 589–598.

Çiftçi, T. D. & Henden, E. 2015 Nickel/nickel boride nanoparticles coated resin: a novel adsorbent for arsenic(III) and arsenic (V) removal. *Powder Technol.* **269**, 470–480.

Erdem, B., Erdem, M. & Özcan, A. S. 2016 Adsorption of Reactive Black 5 onto quaternized 2-dimethylaminoethyl methacrylate based polymer/clay nanocomposites. *Adsorption* **22** (4), 767–776.

Hokkanen, S., Repo, E., Lou, S. & Sillanpää, M. 2015 Removal of arsenic(V) by magnetic nanoparticle activated microfibrillated cellulose. *Chem. Eng. J.* **260**, 886–894.

Jiang, M., Wang, Q., Jin, X. & Chen, Z. 2009 Removal of Pb(II) from aqueous solution using modified and unmodified kaolinite clay. *J. Hazard. Mater.* **170** (1), 332–339.

Kanel, S. R., Grenèche, J.-M. & Choi, H. 2006 Arsenic(V) removal from groundwater using nano scale zero-valent iron as a colloidal reactive barrier material. *Environ. Sci. Technol.* **40** (6), 2045–2050.

Karagöz, S., Tay, T., Ucar, S. & Erdem, M. 2008 Activated carbons from waste biomass by sulfuric acid activation and their use on methylene blue adsorption. *Bioresour. Technol.* **99** (14), 6214–6222.

Lv, X., Xu, J., Jiang, G., Tang, J. & Xu, X. 2012 Highly active nanoscale zero-valent iron (nZVI)-Fe_3O_4 nanocomposites for the removal of chromium(VI) from aqueous solutions. *J. Colloid Interface Sci.* **369** (1), 460–469.

Mahmood, T., Din, S. U., Naeem, A., Mustafa, S., Waseem, M. & Hamayun, M. 2012 Adsorption of arsenate from aqueous solution on binary mixed oxide of iron and silicon. *Chem. Eng. J.* **192**, 90–98.

Manning, B. A., Hunt, M. L., Amrhein, C. & Yarmoff, J. A. 2002 Arsenic(III) and arsenic(V) reactions with zerovalent iron corrosion products. *Environ. Sci. Technol.* **36** (24), 5455–5461.

Monash, P. & Pugazhenthi, G. 2009 Adsorption of crystal violet dye from aqueous solution using mesoporous materials synthesized at room temperature. *Adsorption* **15** (4), 390–405.

Pan, Y.-F., Chiou, C. T. & Lin, T.-F. 2010 Adsorption of arsenic(V) by iron-oxide-coated diatomite (IOCD). *Environ. Sci. Pollut. Res. Int.* **17** (8), 1401–1410.

Pojananukij, N., Wantala, K., Neramittagapong, S. & Neramittagapong, A. 2015 Equilibrium, kinetics, and mechanism of lead adsorption using zero-valent iron coated on diatomite. *Desalin. Water Treat.* **57** (39), 18475–18489.

Prasad, K. S., Gandhi, P. & Selvaraj, K. 2014 Synthesis of green nano iron particles (GnIP) and their application in adsorptive removal of As(III) and As(V) from aqueous solution. *Appl. Surf. Sci.* **317**, 1052–1059.

Singh, T. S. & Pant, K. K. 2004 Equilibrium, kinetics and thermodynamic studies for adsorption of As(III) on activated alumina. *Separ. Purif. Technol.* **36** (2), 139–147.

Straif, K., Benbrahim-Tallaa, L., Baan, R., Grosse, Y., Secretan, B., El Ghissassi, F., Bouvard, V., Guha, N., Freeman, C., Galichet, L. & Cogliano, V. 2009 A review of human carcinogens – Part C: metals, arsenic, dusts, and fibres. *Lancet Oncol.* **10** (5), 453–454.

Tiwari, D. & Lee, S. M. 2012 Novel hybrid materials in the remediation of ground waters contaminated with As(III) and As(V). *Chem. Eng. J.* **204–206**, 23–31.

Vaghetti, J. C. P., Lima, E. C., Royer, B., Brasil, J. L., da Cunha, B. M., Simon, N. M., Cardoso, N. F. & Noreña, C. P. Z. 2008 Application of Brazilian-pine fruit coat as a biosorbent to removal of Cr(VI) from aqueous solution – kinetics and equilibrium study. *Biochem. Eng. J.* **42** (1), 67–76.

WHO 2010 *Guidelines for Drinking-Water Quality*. Available from: www.who.int/water_sanitation_health/dwq/guidelines/en/ (accessed 10 November 2012).

Yan, W., Vasic, R., Frenkel, A. I. & Koel, B. E. 2012 Intraparticle reduction of arsenite (As(III)) by nanoscale zerovalent iron (nZVI) investigated with in situ X-ray absorption spectroscopy. *Environ. Sci. Technol.* **46** (13), 7018–7026.

Yun, D.-M., Cho, H.-H., Jang, J.-W. & Park, J.-W. 2013 Nano zero-valent iron impregnated on titanium dioxide nanotube array film for both oxidation and reduction of methyl orange. *Water Res.* **47** (5), 1858–1866.

Zhang, X., Lin, S., Lu, X.-Q. & Chen, Z. 2010 Removal of Pb(II) from water using synthesized kaolin supported nanoscale zero-valent iron. *Chem. Eng. J.* **163** (3), 243–248.

Zhang, G., Ren, Z., Zhang, X. & Chen, J. 2013 Nanostructured iron (III)-copper(II) binary oxide: a novel adsorbent for enhanced arsenic removal from aqueous solutions. *Water Res.* **47** (12), 4022–4031.

First received 4 April 2016; accepted in revised form 6 July 2016. Available online 3 August 2016